L. H. Rude; U. Filsø; V. D'Anna; A. Stratmann; B. Richter; S. Hino; O. Zavorotynska; M. Baricco; M. H. Sørby; B.C. Hauback; H. Hagemann; F. Besenbacher; J. Skibsted; T. R. Jensen. Hydrogen-fluorine exchange in NaBH4-NaBF4. PHYSICAL CHEMISTRY CHEMICAL PHYSICS. 15 pp: 18185-18194.
DOI: 10.1039/c3cp52815d

Hydrogen–fluorine exchange in $NaBH_4$–$NaBF_4$

L. H. Rude,[a] U. Filsø,[a] V. D'Anna,[b] A. Spyratou,[b] B. Richter,[a] S. Hino,[c]

O. Zavorotynska,[cd] M. Baricco,[d] M. H. Sørby,[c] B. C. Hauback,[c] H. Hagemann,[b] F. Besenbacher,[e] J. Skibsted[f] and T. R. Jensen*[a]

Hydrogen–fluorine exchange in the $NaBH_4$–$NaBF_4$ system is investigated using a range of experimental methods combined with DFT calculations and a possible mechanism for the reactions is proposed. Fluorine substitution is observed using in situ synchrotron radiation powder X-ray diffraction (SR-PXD) as a new Rock salt type compound with idealized composition $NaBF_2H_2$ in the temperature range T = 200 to 215 1C. Combined use of solid-state ^{19}F MAS NMR, FT-IR and DFT calculations supports the formation of a BF_2H_2 complex ion, reproducing the observation of a ^{19}F chemical shift at 144.2 ppm, which is different from that of $NaBF_4$ at 159.2 ppm, along with the new absorption bands observed in the IR spectra. After further heating, the fluorine substituted compound becomes X-ray amorphous and decomposes to NaF at B310 1C. This work shows that fluorine-substituted borohydrides tend to decompose to more stable compounds, e.g. NaF and BF_3 or amorphous products such as closo-boranes, e.g. $Na_2B_{12}H_{12}$. The $NaBH_4$–$NaBF_4$ composite decomposes at lower temperatures (300 1C) compared to $NaBH_4$ (476 1C), as observed by thermogravimetric analysis. $NaBH_4$–$NaBF_4$ (1 : 0.5) preserves 30% of the hydrogen storage capacity after three hydrogen release and uptake cycles compared to 8% for $NaBH_4$ as measured using Sievert's method under identical conditions, but more than 50% using prolonged hydrogen absorption time. The reversible hydrogen storage capacity tends to decrease possibly due to the formation of NaF and $Na_2B_{12}H_{12}$. On the other hand, the additive sodium fluoride appears to facilitate hydrogen uptake, prevent foaming, phase segregation and loss of material from the sample container for samples of $NaBH_4$–NaF.

[a]Center for Materials Crystallography (CMC), Interdisciplinary Nanoscience Center (iNANO) and Department of Chemistry, Aarhus University, Langelandsgade 140,

DK-8000 Aarhus C, Denmark. E-mail: trj@chem.au.dk; Tel: +45 2272 1486

[b]De´partement de Chimie Physique, University of Geneva, 30, quai E. Ansermet, CH1211 Geneva 4, Switzerland

[c] Institute for Energy Technology, Physics Department, P.O. Box 40, Kjeller NO-2027, Norway

[d] Dipartimento di Chimica and NIS, Universita´ di Torino, Torino, Italy

[e] Interdisciplinary Nanoscience Center (iNANO) and Department of Physics and Astronomy, Aarhus University, DK-8000 Aarhus C, Denmark

[f]Instrument Centre for Solid-State NMR Spectroscopy and Interdisciplinary Nanoscience Center (iNANO), Department of Chemistry, Aarhus University, DK-8000 Aarhus C, Denmark

† Electronic supplementary information (ESI) available: DFT results for the isolated ions $BF_{4-x}H_x$ and calculated IR spectra, in situ SR-PXD measurements of $NaBH_4$ and $NaBH_4$–$NaBF_4$ (1 : 0.5, S2). ^{19}F MAS NMR spectra of $NaBH_4$–$NaBF_4$ (1 : 0.5, S2-300). The X-ray diffractogram of $NaBH_4$–$NaBF_4$ (1 : 0.5, S2-300) after NMR measurement. IR measurement of $NaBH_4$–$NaBF_4$ (1 : 0.1, S1), IR spectra of the solid as a function of temperature, TPD-IR spectra as a function of tempera-ture of the released gas, and Sieverts measurements of $NaBH_4$–$NaBF_4$ (1 : 0.5, S2), $NaBH_4$–NaF (1 : 0.25, S6) and $NaBH_4$. Tables with thermal analysis data and Sieverts measurements data. See DOI: 10.1039/c3cp52815d

1 Introduction

Hydrogen has the highest gravimetric energy density but is difficult to store in a compact form, which may be achieved in the solid state.[1–7] Currently, metal borohydride materials are considered promising for hydrogen storage, however, the kinetics and thermodynamics of the hydrogen uptake and release need to be further improved.[8–10] Anion substitution has recently been suggested as a new method to improve the hydrogen storage properties due to possible changes in the lattice energy, chemical pressure and metal–hydrogen bond strength.[8,11] Fluorine substi-tution was reported for sodium hexahydridoalanate, Na_3AlH_6,[12] and ab initio calculations suggest a decreased enthalpy upon substitution, which is verified experimentally.[13,14] Anion substitu-tion in metal borohydride materials was reported for $LiBH_4$–LiX,

where X = Cl, Br, and I in $NaBH_4$–NaCl, in $Ca(BH_4)_2$–CaX_2, X = Cl and I, and in $Mg(BH_4)_2$–MgX_2, X = Cl and Br.[15–24] The change in the hydrogen storage properties of anion-substituted metal borohydride using the heavier halides, Cl, Br or I, is small and may lead to a stabilization, which tends to facilitate hydrogen absorption.[18,19,24] In contrast, calculations reveal that fluorine substitution in $LiBH_4$ is not thermodynamically favored but should indeed provide a destabilization of lithium borohydride.[25,26] Furthermore, fluorine preferably exists on the same boron atom, i.e. formation of one BH_2F_2 is preferred compared to 2 BH_3F .[10,25,27,28] DFT also reveals that room temperature formation of solid solutions between $LiBH_4$ and $LiBF_4$ is not thermodynamically favoured.[25] Experimental reports indicate fluorine substitution in studies of MgB_2–LiF and $LiBH_4$–TiF_3 and also for the KBH_4–KBF_4 system.[29–31]

In this paper, the physical, structural and hydrogen storage properties of the $NaBH_4$–$NaBF_4$ composite are investigated using in situ synchrotron radiation powder X-ray diffraction (SR-PXD), solid-state magic-angle spinning (MAS) NMR spectroscopy, infrared spectroscopy (IR), simultaneous differential scanning calori-metry (DSC), thermogravimetric analysis (TGA), and Sieverts method. DFT calculations on isolated $BF_{4-x}H_x$ ions were also performed and spectral parameters were computed.

2 Experimental section

Sample preparation

Samples of $NaBH_4$–$NaBF_4$ in the molar ratio of 1 : 0.1 and 1 : 0.5, denoted S1 and S2, and reference samples of $NaBH_4$ and $NaBF_4$, denoted R1 and R2, respectively, were ball milled (BM) using the same conditions comprising 15 times 2 min of milling each intervened by 2 min breaks to avoid heating of the samples.[32] Ball milling was conducted under inert conditions in an argon atmosphere with a Fritsch Pulverisette P4 planetary mill using 80 mL tungsten carbide (WC) containers and a sample powder-to-ball mass ratio of approximately 1 : 30 (WC balls, o.d. 10 mm). Fractions, B0.5 g, of the sample $NaBH_4$– $NaBF_4$ (1 : 0.5, S2) were transferred to corundum crucibles, placed in sealed argon-filled quartz tubes, and annealed in a furnace at a fixed temperature. The first sample was annealed at 200 1C for 72 hours and is denoted S2-200. The second and third samples were annealed at 275 and 300 1C, respectively, for 1 hour to analyze the decomposition reaction (S2-275 and S2-300). A hand mixed (HM, B10 min) sample of $NaBH_4$–$NaBF_4$ (1 : 0.5), denoted S3, was prepared using an agate mortar to examine the effect of ball milling. Samples S4 (1 : 1) and S5 (3 : 1) are hand mixed (HM, B10 min), containing physical mixtures of $NaBH_4$ and $NaBF_4$.

Finally, a ball-milled sample of $NaBH_4$–NaF (1 : 0.25) denoted S6 was prepared to investigate the properties of NaF used as an additive. For NMR measurements a sample of NaF was used as received, R3. All samples are listed in Table 1. The chemicals used were: $NaBH_4$ (Z99.99%, Aldrich), $NaBF_4$ (>98%, Aldrich) and NaF (>95%, Aldrich). The preparation and manipulation of all samples were performed in an argon-filled glovebox using a circulation purifier.

Theoretical calculations

Theoretical DFT calculations were performed on the isolated $BH_{4-x}F_x$ ions at B3-LYP/6-31G** level using the Gaussian program[33] with B3-LYP(6-31G**). Isotropic shielding tensors were computed with the Gauge-Independent Atomic Orbital (GIAO) method.[33]

Table 1 List of investigated samples. The composition of the samples is given as relative molar ratios and molar fractions and the theoretical gravimetric hydro-gen content is denoted $r_m(H_2)$. The sample preparation methods are either ball milling (BM) or hand-mixing in a mortar (HM) and in some cases combined with annealing (A) in an argon atmosphere

Notation	Materials	Molar ratio	$n(NaBF_4)$/ n(total)	Preparation	$r_m(H_2)$
S1	$NaBH_4$–$NaBF_4$	1 :0.1	0.091	BM	8.4
S2	$NaBH_4$–$NaBF_4$	1 :0.5	0.334	BM	4.3
S2-200	$NaBH_4$–$NaBF_4$	1 :0.5	0.334	BM, A[b]	4.3
S2-275	$NaBH_4$–$NaBF_4$	1 :0.5	0.334	BM, A[c]	—
S2-300	$NaBH_4$–$NaBF_4$	1 :0.5	0.334	BM, A[d]	—
S3	$NaBH_4$–$NaBF_4$	1 :0.5	0.334	HM	4.3

S4	$NaBH_4$–$NaBF_4$	1 :1	0.500	HM	2.7
S5	$NaBH_4$–$NaBF_4$	1 :0.33	0.250	HM	5.4
S6	$NaBH_4$–NaF	1 :0.25	0.199[a]	BM	6.3
R1	$NaBH_4$	—	—	BM	10.7
R2	$NaBF_4$	—	—	BM	—
R3	NaF	—	—	—	—

[a] n(NaF)/n(total). [b] Annealed at 200 1C for 72 hours. [c] Annealed at 275 1C for 1 hour. [d] Annealed at 300 1C for 1 hour.

Synchrotron radiation powder X-ray diffraction

In situ synchrotron radiation powder X-ray diffraction (SR-PXD) data for sample S2 were measured at beamline BM01A at the Swiss-Norwegian Beam Lines (SNBL), European Synchrotron Radiation Facility (ESRF), Grenoble, France, using a MAR345 image plate detector. The samples were mounted in glass capillaries (0.5 mm o.d.) and sealed to prevent contact with air. The data were collected with a sample-to-detector distance of 250 mm, a 301 rotation of the capillaries during data collection and 30 s X-ray exposure time. The wavelength, l = 0.70082 Å, was calibrated using an external standard, LaB_6. The sample was heated from room temperature (RT) to 450 1C at a heating rate of DT/Dt = 5 1C min ^{1}.

SR-PXD data for sample S2-200 were measured at the MAX-II synchrotron at beamline I711 in the research laboratory MAX-lab, Lund, Sweden using a MAR165 CCD detector system.[34] The sample was mounted in sapphire (Al_2O_3) single crystal tubes (0.79 mm i.d.) in an argon-filled glovebox.[35,36] The experiment was conducted at p(Ar) = 1 bar, in the temperature range from RT to 385 1C (DT/Dt = 5 1C min ^{1}) and l = 0.94499 Å. The data were collected with a sample-to-detector distance of 87 mm, an X-ray exposure time of 30 s per PXD pattern.

The data were integrated using the Fit2D program and analyzed using the Rietveld methods in the FullProf suite.[37,38] The sequential refinement of the in situ SR-PXD data was performed to follow the change in composition and unit cell volumes. The intensity of selected Bragg reflections was integrated and normalized in order to illustrate changes in the sample composition as a function of temperature (the relative amount, $a_i(t) = I_i(t)/I_{i,max}$, of compound i at time t).

Solid-state MAS NMR spectroscopy

Solid-state ^{11}B, ^{19}F and ^{23}Na magic-angle spinning (MAS) spectra were collected for samples S2, S2-275 and S2-300 on a Varian INOVA-400 (9.39 T) spectrometer using a home-built CP/MAS probe for 5 mm o.d. rotors. The ^{19}F MAS NMR spectra were acquired on a Varian INOVA-300 (7.05 T) spectrometer employing the high-frequency $^{1}H/^{19}F$ channel of a home-built CP/MAS NMR probe for 7 mm o.d. rotors. All spectra were obtained at ambient temperature using air-tight end-capped zirconia (PSZ) rotors packed in an argon-filled glovebox.

The ^{11}B, ^{19}F, and ^{23}Na MAS NMR spectra and chemical shifts are referenced to neat $F_3B\ O(CH_2CH_3)_2$, neat CCl_3F, and a 1.0 M aqueous solution of NaCl, respectively. Simulations and least-squares fitting of the ^{23}Na MAS NMR spectra were performed using the STARS simulation software package.[39]

Thermal analysis

Differential scanning calorimetry (DSC) and thermogravimetric analysis (TGA) were performed simultaneously using a Netzsch STA449C Jupiter instrument at a heating rate of 5 1C min ^{1} from RT to 450 1C (S2 and S3) or to 600 1C (S1, R1 and R2) in a flow of He (50 mL min ^{1}). The samples were placed in Al_2O_3 crucibles with a small hole in the lid to prevent the increase of pressure.

Mass spectroscopy

The gas release from the samples of $NaBH_4$–$NaBF_4$ (1 : 0.1, S1) and $NaBH_4$–$NaBF_4$ (1 : 0.5, S2) was investigated using a MKS Microvision-IP residual gas analyzer (RGA) by mass spectroscopy (MS) attached to an in-house-built temperature-programmed desorption (TPD) setup. The sample was contained in a stainless-steel autoclave and heated from RT to 600 1C (DT/Dt = 2 1C min ^{1}) under dynamic vacuum. The pressure in the autoclave was measured using an Alcatel ACC 1009 vacuum gauge. The ratios of selected gas components (H_2, B_2H_6, and BF_3) were roughly estimated from peak area of calibrated mass spectra. The calibra-tion was performed using $NaAlH_4$ and $NaBF_4$ as sources of H_2 and BF_3 gases, respectively, to determine the linear relationship between the MS signal and pressure for each gas species. The coefficient for the B_2H_6 spectrum was determined by fitting the sum of these calibrated spectra with the total pressure. Due to fragmentation of the gas molecules during ionization, the most intense signals from B_2H_6 and BF_3 were mass 26 ($B_2H_4^+$) and 49 (BF_2^+) and these signals were used for the analysis.

Infrared spectroscopy

Gas-infrared (IR) spectroscopy measurements were performed using a Vertex 70 FT-IR spectrometer (Bruker Optics) in the range 4000 to 600 cm ^{1} with 0.5 cm ^{1} resolution. The sample holder was connected to the gas IR cell and the set-up was degassed to 10 ^{5} mbar. IR spectra of the evolved gases were recorded while continuously heating the sample in a closed system from RT to 300 1C (DT/Dt = 3 1C min ^{1}) and then at a constant temperature of 300 1C for about 1 hour. The sample $NaBH_4$–$NaBF_4$ (1 : 0.1, S1, 0.083

g) was placed in a quartz tube under an argon atmosphere. After the experiment, the residual sample mass was 0.072 g corresponding to a mass loss of 0.011 g or ca. 13 wt%. Molecular H_2 is IR inactive and the measurement aimed to detect other gases such as boranes or BF_3. A negative signal is recorded in the 1800–1600 cm ^{1} region corresponding to the water vapor of the background.

Temperature-dependent FTIR experiments on solid samples were performed using a BioRad Excalibur Instrument equipped with a Specac Golden Gate heatable ATR set-up. The spectral resolution was set to be 1 cm ^{1}.

Sieverts measurements

Sieverts-type measurements were performed for samples of $NaBH_4$–$NaBF_4$ (1 : 0.5, S2) and $NaBH_4$ (R1) using a PCTpro 2000 instrument from Hy-Energy.[40] The samples were loaded in an autoclave and sealed in an argon atmosphere. The Sieverts-type desorption experiments were performed at $p(H_2)$ = 1 bar from RT to 300 1C (DT/Dt = 4 1C min ^{1}), followed by constant temperature T = 300 1C for 2 h, heating from 300 to 550 1C (DT/Dt = 4 1C min ^{1}) and prolonged annealing at T = 550 1C. Hydrogen absorptions were conducted at a fixed temperature of 450 1C for 24 hours at $p(H_2)$ = 130 bar.

3 Results and discussion

Theoretical calculations

DFT calculations on all 5 isolated $BH_{4\ x}F_x$ ions (x = 0 to x = 4) showed that these ions are stable, i.e. no imaginary vibrational frequency was found. The corresponding bond length and angles, the calculated IR spectra as well as the computed isotropic magnetic shielding tensor values are given in the ESI,† Tables S1–S3 and Fig. S1. The total energy (zero point corrected energy) is computed for the $BH_{4\ x}F_x$ ions (x = 0 to x = 4), which can be used to estimate the reaction energy (at 0 K) for reaction (1).

$$aBH_4 + bBF_4 - BH_{4\ x}F_x \quad (a + b = 1) \qquad (1)$$

The calculated reaction energy for the formation of the ions BH_3F , BH_2F_2 and BHF_3 was 52, 54 and 28 kJ mol ^{1}, respectively. The results indicate that the formation of all mixed hydrogen–fluorine compounds is significantly endothermic (up to ca. 55 kJ mol ^{1}).

In situ SR-PXD

The samples of $NaBH_4$–$NaBF_4$ (1 : 0.5, S2 and 1 : 0.5, S2-200) were studied using in situ SR-PXD in the temperature range from RT to 385 1C. The first diffractogram in Fig. 1a measured at 23 1C for sample $NaBH_4$–$NaBF_4$ (1 : 0.5, S2-200) reveals Bragg diffraction peaks from $NaBH_4$ and o-$NaBF_4$. This suggests that no reaction occurred during ball milling and thermal activation of sample S2-200 (200 1C/72 h) prior to the SR-PXD analysis. During heating, the transformation from orthorhombic o-$NaBF_4$ to hexagonal h-$NaBF_4$ polymorphs is observed at 221 1C, in accor-dance with previous studies where this transition was observed at 227 1C.[41] The Bragg reflections from h-$NaBF_4$ disappear at 273 1C, which is significantly lower than the reported melting point, $T_{mp}(NaBF_4)$ = 357 1C.[41] The diffracted intensity from $NaBH_4$ continuously decreases during heating from RT to B211 1C due to increasing thermal vibrations in the material. This is also observed for $NaBH_4$ (R1), see Fig. S2 in the ESI.† $NaBH_4$ in sample S2-200 decomposes between 211 and 320 1C, which is a significantly lower temperature than the range B450 to 500 1C observed for $NaBH_4$ (R1), see Fig. S2 (ESI†). Formation of NaF is observed in the temperature range 269 to B350 1C. Integrated, normalized diffracted intensities for selected well-resolved reflections from the observed compounds are visualized in Fig. 1b. The transformation from o- to h-$NaBF_4$ at 221 1C is fast and the decomposition of h-$NaBF_4$ is almost equally fast. Interestingly, the onset of sodium fluoride, NaF, formation occurs when almost all h-$NaBF_4$ is decomposed leaving a ‘gap’ with limited amounts of crystalline material in the sample. This suggests the presence of amorphous intermediates during decomposition of $NaBH_4$–$NaBF_4$.

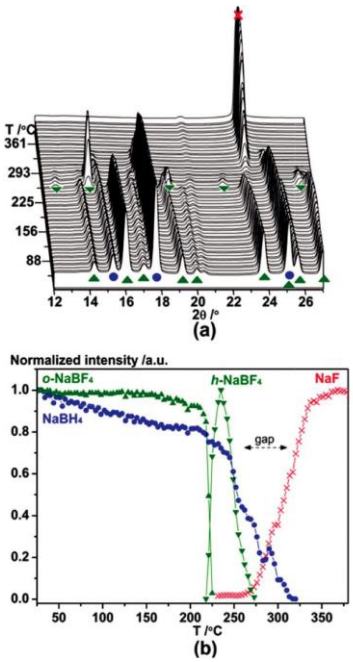

Fig. 1 In situ SR-PXD data (a) measured for $NaBH_4$–$NaBF_4$ (1 : 0.5, S2-200) in the temperature range of RT to 385 1C with DT/Dt = 5 1C min ^{1}, l = 0.94499 Å, using beam line I711 at MAX-lab. (b) Normalized integrated diffracted intensities for the crystalline compounds in the sample. Symbols: K $NaBH_4$; m o-$NaBF_4$;. h-$NaBF_4$; NaF.

In a similar in situ SR-PXD study of $NaBH_4$–$NaBF_4$ (1 : 0.5, S2) the same 'gap' was observed during decomposition, see Fig. S3 (ESI†). However, after disappearance of diffraction from h-$NaBF_4$ a few of the following diffractograms contain Bragg peaks from a new compound. Numerous diffraction experiments were conducted, also with other sample compositions not included in this publication, but only in one case was the new set of diffraction peaks is sufficiently intense to allow indexation (Fig. 2 and Fig. S3, ESI†), using a cubic unit cell, a = 6.7616(6) Å

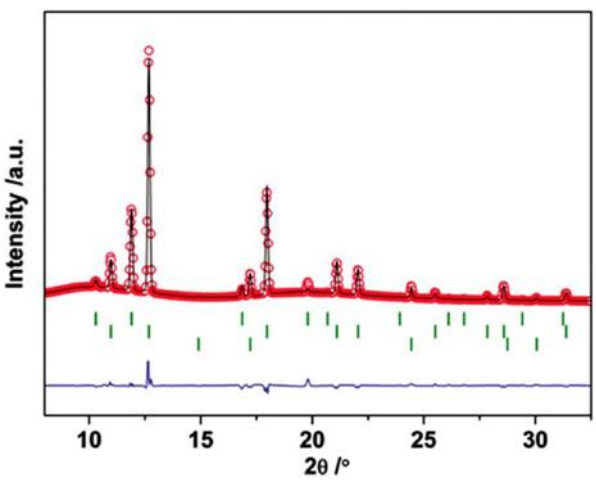

Fig. 2 Rietveld refinement of the in situ data of $NaBH_4$–$NaBF_4$ (1 : 0.5, S2) collected at T = 208 1C with l = 0.70082 Å. Symbols: observed data (red circles), calculated fit (black line) and the difference plot (blue line). Green tick marks indicate reflections from $NaBH_{2.1}F_{1.9}$ (top), $NaBH_4$ (mid) and NaF (bottom).

(V = 309.13(4) Å^3, and possible space group Fm3%m). Thus, this compound may have a Rock salt type structure isomorphous to $NaBH_4$ but with a larger unit cell volume. A structural model for Rietveld refinement was constructed with fluorine and hydrogen statistically distributed on the same position as hydrogen in the $NaBH_4$ structure. The refined composition is $NaBH_{2.1}F_{1.9}$ (at T = 208 1C, see Fig. 2) in agreement with a unit cell volume increase of 21.0% (V/Z = 77.3 Å^3) compared to that for $NaBH_4$ (V/Z = 63.9 Å^3, T = 208 1C) and a decrease of 7.4% compared to $NaBF_4$ (V/Z = 83.5 Å^3, T = 207 1C).[41] In fact, the unit cell volume for $NaBH_4$ in sample S2 (see Fig. 2) is slightly larger than the value for pristine $NaBH_4$ (V/Z = 61.1 Å^3 at T = 210 1C, see Fig. S2, ESI†). However, the fluorine substitution appears to be within the experimental uncertainty and cannot be estimated accurately.

NMR spectroscopy

The ^{11}B MAS NMR spectrum of the central and satellite transi-tions for the $NaBH_4$–$NaBF_4$ (1 : 0.5, S2) sample before heating (Fig. 3a) contains two sets of resonances with centerbands at d(^{11}B) = 1.7 ppm and d(^{11}B) = 41.9 ppm, corresponding to the isotropic chemical shifts of $NaBF_4$ and $NaBH_4$, respectively.[42,43] The centerband from $NaBH_4$ exhibits a linewidth of FWHM = 0.6 ppm in the ^{1}H decoupled ^{11}B MAS spectrum (Fig. 3a), whereas it is somewhat larger (FWHM = 3.2 ppm) for the $NaBF_4$ centerband. Integration of all resonances from the central and satellite transitions for the two compounds gives a $NaBH_4$– $NaBF_4$ intensity ratio of 1.0 : 0.37 which is in fair agreement with the reactant ratio used in the preparation of the sample $NaBH_4$–$NaBF_4$ (1 : 0.5, S2). This result shows that no reaction occurs during ball milling of the $NaBH_4$–$NaBF_4$ mixture, in agreement with the X-ray diffraction results.

The ^{11}B MAS NMR spectrum of sample S2-300 after heat treatment (300 1C for 1 hour) is shown in Fig. 3b and exhibits resonances from $NaBF_4$, $NaBH_4$ and a new compound with a centerband resonance at d(^{11}B) = 15.5 ppm which is assigned (FWHM = 3.6 ppm) and NaF, d(^{19}F) = 222.8 ppm (FWHM = 7.9 ppm). This is apparent from a comparison of the spectrum in Fig. S5a (ESI†) with a similar ^{19}F MAS NMR spectrum acquired for $NaBF_4$ (Fig. S5b, ESI†) and the chemical shift value, d(^{19}F) = 221 ppm, reported for NaF.[46] An analysis of the intensities for the partly overlapping centerbands and spinning sidebands in the ^{19}F MAS NMR spectrum (Fig. S5a, ESI†) gives a ^{19}F intensity ratio of 1.0 : 0.49 for $NaBF_4$ and NaF, corresponding to a sample composition with a $NaBF_4$: NaF molar ratio of 1.0 : 1.95.

The ^{23}Na spectrum of the $NaBH_4$–$NaBF_4$ (1 : 0.5, S2) sample (Fig. 4a) includes a narrow central-transition centerband from $NaBH_4$ at 8.4 ppm (FWHM = 1.2 ppm) and a partly resolved second-order quadrupolar lineshape at about 20 ppm from $NaBF_4$ (Fig. 4c).[41,47] ^{23}Na MAS NMR spectra of the central and satellite transitions for samples of $NaBH_4$ and $NaBF_4$ have been acquired (not shown), which allow determination of the ^{23}Na isotropic chemical shifts and quadrupole coupling parameters (Table 2) from simulations and least-squares fitting to the spinning sidebands from the satellite transitions.[39] The quad-rupole coupling parameters for $NaBF_4$ (Table 2) are in good agreement with earlier reported parameters (C_Q = 1008.4 kHz and Z_Q = 0.095) determined from ^{23}Na single-crystal NMR at 23 1C.[48] Moreover, the ^{23}Na data determined for $NaBH_4$

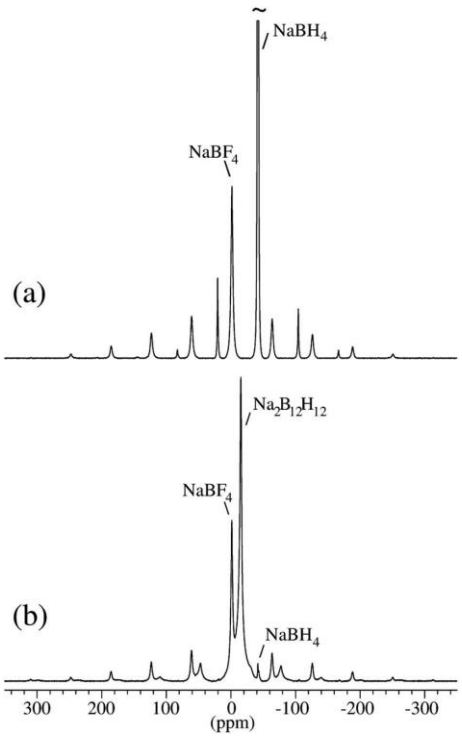

Fig. 3 ^{11}B MAS NMR spectra of the central and satellite transitions for (a) $NaBH_4$– $NaBF_4$ (1 : 0.5, S2) and (b) $NaBH_4$–$NaBF_4$ (1 : 0.5, S2-300) after heating to T = 300 1C for 1 h. The spinning sidebands from the satellite transitions associated with the centerband resonance at 15.5 ppm extend further than the selected spectral region shown in the figure. Both ^{11}B MAS NMR spectra have been acquired at 9.4 T with ^{1}H decoupling and a spinning speed of n_R = 8.0 kHz, using a short excita-tion pulse (t_p = 0.5 ms) and a relaxation delay of 30 s. The narrow resonance at 41.9 ppm from $NaBH_4$ is cut-off at 1/2 of its total height in (a).to $Na_2B_{12}H_{12}$ on the basis of the recently reported ^{11}B chemical shift (d(^{11}B) = 15.4 ppm, 9.4 T) for this compound.[44] The centerband resonance from $Na_2B_{12}H_{12}$ at d(^{11}B) = 15.5 ppm is slightly broader (FWHM = 3.4 ppm) than the centerband of $NaBF_4$ (FWHM = 3.1 ppm) and much broader than the center-band from $NaBH_4$ (FWHM = 0.7 ppm).

Examination of the intensities for the central-transition centerbands reveals relative ^{11}B intensities of 0.26 : 0.72 : 0.02 for $NaBF_4$, $Na_2B_{12}H_{12}$, and $NaBH_4$, corresponding to the molar ratios of 0.26 : 0.06 : 0.02, respectively, indicating that $Na_2B_{12}H_{12}$ is the principal decomposition product of the S2-300 sample. PXD data measured for sample S2-300 only reveal Bragg reflec-tions from $NaBF_4$ and NaF (see Fig. S4, ESI†), which suggest that $Na_2B_{12}H_{12}$ and the small amount of $NaBH_4$ are X-ray amorphous, similar to amorphous $LiBH_4$ observed by ^{11}B MAS NMR in a study of $Y(BH_4)_3$.[45]

The above-mentioned results are in accordance with the ^{19}F MAS NMR spectrum of the S2-300 sample (Fig. S5a, ESI†), which only includes resonances from $NaBF_4$, d(^{19}F) = 159.2 ppm agree well with the quadrupole coupling parameters reported recently from static-powder ^{23}Na NMR experiments (C_Q = 0.154 0.003 MHz, Z_Q = 0.10 0.05).[49] The ^{23}Na MAS NMR spectrum of the sample S2-300 (Fig. 4b) shows clearly that all $NaBH_4$ has decomposed and that NaF (Fig. 4d) is the principal sodium-containing compound after the heat treatment. The absence of $NaBH_4$ is in accord with the corresponding ^{11}B MAS NMR spectrum (Fig. 3b) which only contains a very low-intensity peak from $NaBH_4$ (2% intensity). In addition, a centerband resonance at 17.4 ppm is observed, which partly overlaps with the central transition from $NaBF_4$. This resonance is assigned to X-ray amorphous $Na_2B_{12}H_{12}$, following the observation of this phase in the ^{11}B NMR spectrum (Fig. 3b, d(^{11}B) = 15.5 ppm).

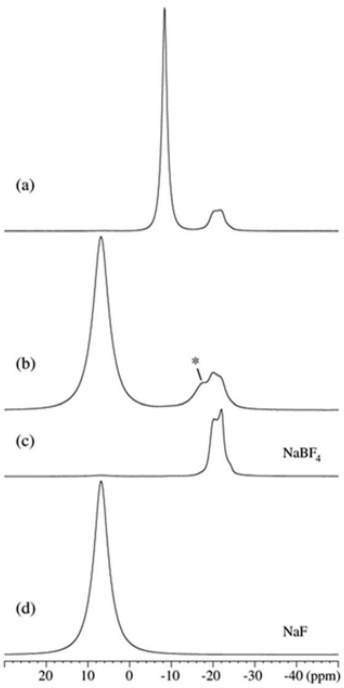

Fig. 4 ^{23}Na MAS NMR spectra (9.4 T, n_R = 10.0 kHz, t_p = 0.5 ms), illustrating the central-transition region for (a) $NaBH_4$–$NaBF_4$ (1 : 0.5, S2), (b) $NaBH_4$–$NaBF_4$ (1 : 0.5, S2-300) after heating to T = 300 1C for 1 h and for samples of (c) $NaBF_4$ and (d) NaF. The spectra in (a) and (b) employed ^{1}H decoupling during acquisi-tion. The asterisk in (b) indicates the centerband from the $Na_2B_{12}H_{12}$ decom-position product.

Table 2 ^{23}Na isotropic chemical shifts and quadrupole coupling parameters for $NaBH_4$ and $NaBF_4$ determined from ^{23}Na MAS NMR spectra of the central and satellite transitions

	d_{iso}[a]/ppm		C_Q[b]/MHz		Z_Q[b]	
$NaBH_4$	8.4	0.2	0.147	0.002	0.08	0.01
$NaBF_4$	18.6	0.2	0.998	0.002	0.08	0.01

[a] ^{23}Na isotropic chemical shift relative to a 1.0 M aqueous solution of NaCl. [b] The quadrupole coupling parameters are defined as $C_Q = (eQ/h)V_{zz}$ and $Z_Q = (V_{yy} V_{xx})/V_{zz}$, where V_{ii} are the principal elements of the electric field gradient tensor following the definition: $|V_{zz}| Z |V_{xx}| Z |V_{yy}|$, Q is the nuclear electric quadrupole moment of ^{23}Na and e, the charge of the electron.

The sample S2 heat-treated at 275 1C (S2-275) has also been characterized by ^{11}B, ^{19}F, and ^{23}Na MAS NMR. The ^{23}Na MAS NMR spectrum (not shown) is dominated by the resonances from $NaBH_4$ and $NaBF_4$ in an approximate 2 : 1 ratio. Only a low-intensity resonance from NaF is observed, constituting 3.5% of the total central-transition intensities, thereby demon-strating that only a minor part of the sample has decomposed by heat-treatment at 275 1C. This is also apparent from the ^{11}B MAS NMR spectrum (Fig. 5a), which is dominated by the centerbands and spinning sidebands from $NaBH_4$ and $NaBF_4$. However, a very low-intensity (B0.004%) centerband at d(^{11}B) = 15.5 ppm from $Na_2B_{12}H_{12}$ can also be identified. More inter-estingly, the ^{19}F MAS NMR spectrum of the S2-275 sample (Fig. 5b) clearly reveals the presence of two new fluorine environments by the resonances at d(^{19}F) = 144.2 ppm and 150.6 ppm in addition to the dominating peak at d(^{19}F) = 159.2 ppm from $NaBF_4$. The new resonances are ascribed to fluorine that substitutes for hydrogen in the BH_4 units of $NaBH_4$. The SCF GIAO calculated isotropic ^{19}F magnetic shield-ing tensor yields a value of 360.5 ppm (absolute shielding) for fluorine in BF_4 , and a value of 376.8 ppm for fluorine in BF_2H_2 , corresponding to a positive shift of ca. 16 ppm (see Table S3, ESI†), similar to the one observed experimentally. In contrast, the calculated isotropic ^{11}B isotropic shifts for BF_4 , BF_3H and BF_2H_2 only exhibit a 3 ppm variation, which is within the experimental resolution, considering the line-widths of the centerband resonances. Thus, BF_4 , BF_3H and BF_2H_2 cannot be distinguished experimentally under the ^{11}B MAS NMR conditions used here.

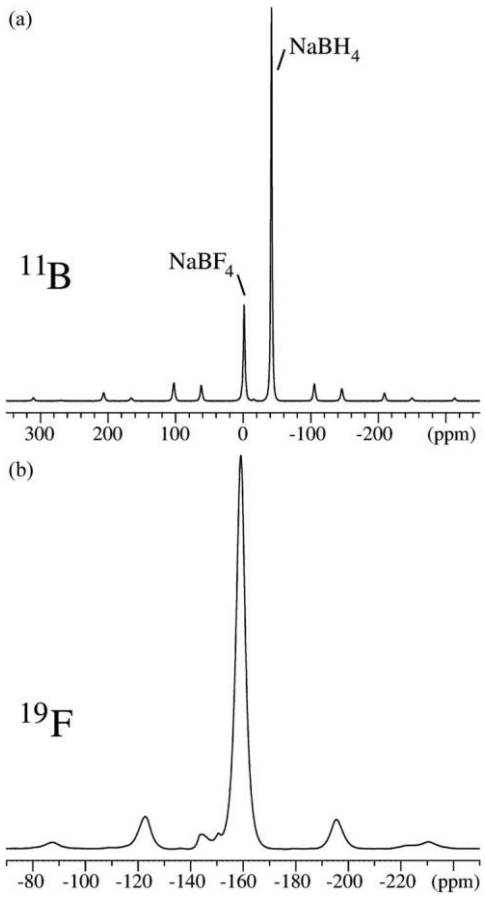

Fig. 5 ^{11}B and ^{19}F MAS NMR spectra (7.1 T, n_R = 10.0 kHz) of $NaBH_4$–$NaBF_4$ (1 : 0.5) after heating to T = 275 1C for 1 h (S2-275), obtained with relaxation delays of 10 s and 8 s, respectively.

Temperature-dependent infrared spectroscopy

The samples of $NaBH_4$–$NaBF_4$ (1 : 1, S4) and $NaBH_4$–$NaBF_4$ (1 : 0.33, S5) were studied using FT-IR as a function of increas-ing temperature with steps of 10 1C from RT to 280 1C and then cooled to RT (see Fig. S6 and S7, ESI†). The initial spectra suggest the presence of a physical mixture, as no new bands besides those of $NaBH_4$ and $NaBF_4$ are observed (Fig. S8, ESI†). Upon heating, new bands at ca. 800 and 1200 cm ^{1} are observed at T > 230 1C. Fig. S9 (ESI†) compares the spectra of the sample $NaBH_4$–$NaBF_4$ (1 : 1, S4) measured at RT and after heating to 280 1C.

As a consequence, new bands are observed at 792, 900, 1198 and 1248 cm ^{1}. Besides the band at 792 cm ^{1}, all other new bands fall in the range of the frequencies calculated (for gaseous molecules) for intermediate $BH_4{}_xF_x$ ions (see Fig. S9, ESI†), supporting the conclusions from the NMR experiments. It is interesting to note that the B–H stretching mode region (between 2000 and 2500 cm ^{1}) does not appear to be strongly changed by the heat treatment. Note that the B–H stretching modes are subject to strong Fermi resonances, making it difficult to analyze this spectral region.[50] The results for the 1 : 0.33 mixtures are similar to those of the 1 : 1 mixture (see Fig. S6 and S7, ESI†).

Residual gas analysis

The gas released from samples of $NaBH_4$–$NaBF_4$ (1 : 0.1, S1) and $NaBH_4$–$NaBF_4$ (1 : 0.5, S2) was investigated by TPD-MS in the temperature range RT to 600 1C, see Fig. 6. $NaBH_4$ (R1) and $NaBF_4$ (R2) were also measured as references and a zoom (intensity 10) of Fig. 6a is provided in Fig. S12 (ESI†). The TPD-MS of $NaBH_4$ reveals hydrogen release in two steps, at T = 476 and 519 1C, respectively. The TPD-MS spectrum of $NaBF_4$ shows release of BF_3 at 398 1C. A large H_2-signal with a peak temperature of 305 1C is observed for sample S2. Mass fragments of B_2H_6 and BF_3 were also detected in the same temperature range, see Fig. 6a. The integrals of the calibrated MS profiles can be used to estimate the relative amounts of the gases released. Sample $NaBH_4$–$NaBF_4$ (1 : 0.5, S2) releases B92% H_2 together with minor fractions of B_2H_6 (B3%) and BF_3 (B5%).

For sample $NaBH_4$–$NaBF_4$ (1 : 0.1, S1) the relative amounts of H_2, B_2H_6, and BF_3 are 88, 4 and 8%, respectively. However, a major part of hydrogen is released at 483 1C while B_2H_6 and BF_3 are detected at 277 1C, see Fig. 6b. Interestingly, this hydrogen release is observed at reduced temperatures, B50 1C below pristine $NaBH_4$. A MS signal corresponding to the mixed fluorine–hydrogen ion (BFH^+, m/z = 31) is also detected in both samples, which may indicate decomposition of B–H–F containing compounds in the samples.

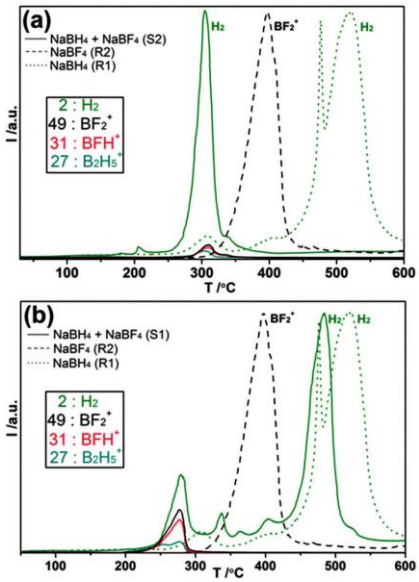

Fig. 6 TPD-MS measurements performed in the temperature range from RT to 600 1C (DT/Dt = 2 1C min ^{1}) for samples (a) $NaBH_4$–$NaBF_4$ (1 : 0.5, S2) and (b) $NaBH_4$–$NaBF_4$ (1 : 0.1, S1). For comparison, both figures show data for the individual compounds $NaBH_4$ (R1) and $NaBF_4$ (R2). The mass fragments detected correspond to H_2, B_2H_6, and BF_3.

Infrared spectra of the gases evolved during decomposition of the $NaBH_4$–$NaBF_4$ (1 : 0.1, S1) and $NaBH_4$–$NaBF_4$ (1 : 0.5, S2) samples were measured, see Fig. S10 and S11 (ESI†). The first IR signal appeared when the gas concentration in the cell was sufficient to reach the instrument sensitivity, which depends on the absorbance coefficient of each gas. The first signals for BF_3 and B_2H_6 were recorded at 90 1C, which means that desorption of these species started just below this temperature.

Thermal analysis

DSC and TGA measurements were conducted for $NaBH_4$–$NaBF_4$ (1 : 0.1, BM, S1), (1 : 0.5, BM, S2) and (1 : 0.5, HM, S3) and are compared with results for $NaBH_4$ (R1) and $NaBF_4$ (R2) (Fig. 7). The data were collected at temperatures from RT to above 450 1C (heating rate 5 1C min ^{1}) and the results are listed in Table S4 (ESI†).

The DSC profile of $NaBH_4$ (R1) shows endothermic signals at T = 484 and B540 1C assigned to melting and decomposition. The corresponding TGA mass loss (28 wt%, observed) between 477 and 600 1C is larger than the gravimetric hydrogen content of $NaBH_4$, r_m = 10.7 wt% H_2, which may be due to melting and foaming of $NaBH_4$ during decomposition resulting in loss of

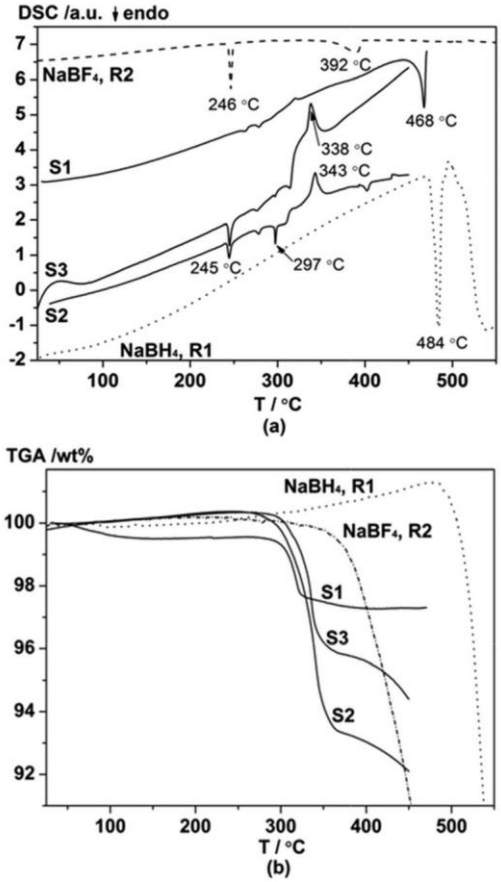

Fig. 7 (a) Differential scanning calorimetry (DSC) conducted from RT to >450 1C (DT/Dt = 5 1C min ^{1}) for $NaBH_4$–$NaBF_4$ (1 : 0.1, BM, S1), (1 : 0.5, BM, S2), (1 : 0.5, HM, S3), $NaBH_4$ (R1), and for $NaBF_4$ (R2). (b) Thermogravimetric analysis (TGA) conducted simultaneously with the DSC. The weight loss observed for samples S1–S3 at T o 380 1C appears to be related to the exothermic signal in the DSC.

material and possibly also decomposition of sodium hydride, NaH, and evaporation of sodium according to reaction scheme (1).[51,52]

$$NaBH_4(l) - Na(l,g) + B(s) + 2H_2(g) \qquad (2)$$

The DSC profile of $NaBF_4$ (R2) reveals an endothermic signal at T = 246 1C assigned to the o- to h-$NaBF_4$ polymorphic transformation. A broad endothermic signal with peak intensity at T = 392 1C is associated with an observed mass loss of 33 wt% observed from 392 to 600 1C. Full decomposition of $NaBF_4$ to NaF and BF_3 according to reaction scheme (3) corresponds to a calculated mass loss of $Dm/m(BF_3)$ = 61.8 wt%, which occurs at temperatures above the melting point, $T_{mp}(NaBF_4)$ = 357 1C.[41]

$$NaBF_4(l) - NaF(s) + BF_3(g) \qquad (3)$$

The DSC profile of $NaBH_4$–$NaBF_4$ (1 : 0.1, S1) shows weak endothermic signals at T = 263 and 278 1C, assigned to decomposition as observed by TPD-MS. A TGA mass loss of 2.3 wt% is recorded in the temperature range 300 to 320 1C. At 321 and 468 1C a weak exothermic and a stronger endothermic event is recorded and assigned to the formation of $Na_2B_{12}H_{12}$ and the melting of excess $NaBH_4$, respectively. For $NaBH_4$– $NaBF_4$ (1 : 0.5, BM, S2) and (1 : 0.5, HM, S3) endothermic signals are observed at T = 245, 278 and 297 1C for both samples and also at 314 1C for S3. The first endothermic event is assigned to the o- to h-$NaBF_4$ polymorphic transformation whereas the second event, at T = 278 1C, cannot directly be coupled with any reaction observed by in situ SR-PXD involving crystalline reactants. The endothermic events at 297 and 314 1C are corre-lated with the mass loss observed in the temperature range 300 to 350 1C of 7.0 and 4.5 wt% for S2 and S3, respectively, and also to the significant release of hydrogen detected by TPD-MS. A broad exothermic signal observed in the temperature range B315 to B350 1C with a peak value at T B 340 1C may be assigned to multiple reactions in the sample, e.g. formation of $Na_2B_{12}H_{12}$. The DSC and TGA profiles of the ball-milled and physically mixed samples of $NaBH_4$–$NaBF_4$ (1 : 0.5, BM, S2 and 1 : 0.5, HM, S3) are similar, but also reveal some differences, e.g. more solid-state chemical reactions in the HM sample in the temperature range B315 to 350 1C are stronger, which lead to a smaller mass loss.

Sieverts measurements

The reversible hydrogen storage properties of $NaBH_4$–$NaBF_4$ (1 : 0.5, S2) were investigated using the Sieverts approach, see Fig. S13 and Table S5 (ESI†). During the first desorption $NaBH_4$–$NaBF_4$ (1 : 0.5, S2) releases 9.1 wt% H_2–$NaBH_4$ and 3.6 and 3.2 wt% H_2–$NaBH_4$ during the second and third desorption, respectively. Thus, the reversible capacity of the system $NaBH_4$– $NaBF_4$ appears to be improved as compared to $NaBH_4$ (R1) used as a reference. $NaBH_4$ (R1) releases 6.0 wt% H_2 during 105 h (the first 12 h are shown in Fig. S13, ESI†) corresponding to 56% of the theoretical hydrogen capacity $r_m(H_2)$ = 10.7 wt%, assuming formation of NaH. Complete dehydrogenation requires higher temperatures due to the back pressure of $p(H_2)$ = 1 bar used during desorption. Rehydrogenation was performed at T = 450 1C, $p(H_2)$ B 130 bar for 24 h, but the second and third dehydrogenation only release 0.69 and 0.65 wt% H_2, i.e. B6% of the theoretical capacity. $NaBH_4$ is expected to absorb hydrogen at higher temperatures, 550 to 700 1C.[51] Recent research shows that addition of nano-porous carbon facilities hydrogen uptake for bulk $NaBH_4$ significantly.[53]

In order to address the possible effect of sodium fluoride, NaF, on the hydrogen storage properties a sample of $NaBH_4$–NaF (1 : 0.25, S6) was investigated. The first desorption of S6 resembles pure $NaBH_4$ with a total gas release of 4.9 wt% and 1.1 wt% in both second and third desorption, see Fig. S14 (ESI†). Thus, NaF appears to have a positive effect on hydrogen adsorption in $NaBH_4$ possibly by limiting the formation of foam and phase segregation and possibly also influenced by H–F exchange in $NaBH_4$.[52]

The mechanism for hydrogen–fluorine exchange

Hydrogen release from metal borohydrides is strongly dependent on the gas pressure.[54,55] Decomposition of $NaBH_4$ at $p(H_2)$ B 0 in the TGA experiment resulted in loss of the sample possibly by 'foaming', whereas a slow loss of 6 wt% H_2 over 105 h was observed at $p(H_2)$ B 1 bar using the Sieverts method. Furthermore, the results presented here suggest that utilization of sodium fluoride as an additive may eliminate foaming of the sample.

A possible reaction mechanism for hydrogen–fluorine exchange in the $NaBH_4$–$NaBF_4$ system may be suggested based on the results presented in this paper. $NaBH_4$–$NaBF_4$ samples generally reveal decreasing amounts of crystalline material in the temperature range B250 to 310 1C, observed as a 'gap' in the diffraction data. In a few cases, weak diffraction from a new compound with the idealized composition, '$NaBF_2H_2$', was observed, which may form according to reaction (4).

$$NaBH_4(s) + NaBF_4(s) - 2NaBF_2H_2(s) \quad (4)$$

This new compound may account for the ^{19}F NMR resonance observed at 144.2 ppm, shifted to higher frequency relative to $NaBF_4$ ($d(^{19}F)$ = 159.2 ppm). This is further supported by the SCF GIAO calculations which predict a 16 ppm shift to a higher frequency for a BF_2H_2 unit relative to a BF_4 site.

Reaction (4) may occur in the phase boundary between individual $NaBH_4$ and $NaBF_4$ particles. This hydrogen–fluorine exchange reaction (4) may be the first of multiple reactions, which lead to amorphous products. The product from (4) may react with excess sodium borohydride and form diborane, B_2H_6, and the stable and inert salt sodium fluoride according to in situ SR-PXD data, see reaction (5).

$$NaBH_4(s) + NaBF_2H_2(s) - B_2H_6(g) + 2NaF(s) \quad (5)$$

$$2NaBH_4(s) + 5B_2H_6(g) - Na_2B_{12}H_{12}(s) + 13H_2(g) \quad (6)$$

The formed diborane may react with sodium borohydride and polymerize to the more stable closo-boranes, e.g. $Na_2B_{12}H_{12}$, see reaction (6). In fact, reactions (4)–(6) can be added to give the overall reaction (7).

$$9.5NaBH_4(s) + 2.5NaBF_4(s) - Na_2B_{12}H_{12}(s) + 10NaF(s) + 13H_2(g) \quad (7)$$

Reaction (7) corresponds to a hydrogen mass loss of $r_m(H_2)$ = 4.31 wt% H_2 and tends to suggest that >21 mol% $NaBF_4$ in

samples of $NaBH_4$–$NaBF_4$ corresponds to excess $NaBF_4$ and may lead to release of BF_3, as shown in eqn (3). The TGA results are in good agreement with reaction (7), i.e. sample $NaBH_4$– $NaBF_4$ (1 : 0.1, S1) releases half of this amount of gas, whereas S2 (0.666 : 0.334) releases slightly more. Interestingly, the major hydrogen release from $NaBH_4$–$NaBF_4$ (1 : 0.1, S1) is observed at significantly lower temperatures, B50 1C, as compared to $NaBH_4$. A drawback for the $NaBH_4$–$NaBF_4$ composite is the formation of stable closo-boranes, e.g. $Na_2B_{12}H_{12}$, which are generally considered difficult to rehydrogenate.[56,57]

4 Conclusions

Direct observation of hydrogen–fluorine substitution in metal borohydrides was performed using in situ SR-PXD as a new Rock salt type compound with idealized composition $NaBF_2H_2$. Combined use of solid-state ^{19}F MAS NMR and DFT calcula-tions confirms the formation of a BF_2H_2 complex ion, which is also supported by combined use of FT-IR and DFT. This work shows that fluorine substituted borohydrides appear to be relatively unstable and tend to decompose to more stable compounds, e.g., the ionic compound NaF and the covalent, molecular BF_3 gas or amorphous products such as closo-boranes, e.g. $Na_2B_{12}H_{12}$. H–F exchange appears to be facilitated by less stable fluorine containing reactants (i.e. $NaBF_4$) as compared to the more stable reaction products formed during decomposi-tion. The $NaBH_4$–$NaBF_4$ composite decomposes at lower tem-peratures (T B 300 1C) compared to $NaBH_4$ (T = 476 1C), preserves 30% of the hydrogen storage capacity after three hydrogen release and uptake cycles compared to 6% for $NaBH_4$ and more than 50% using prolonged absorption time. Thus, this work demonstrates that hydride–fluoride exchange in hydrogen storage materials may significantly change the phy-sical properties. H–F exchange may facilitate hydrogen uptake, prevent foaming, phase segregation and loss of material during release of hydrogen by thermolysis. Furthermore, lightweight fluoride-containing materials are of increasing interest for other energy-related purposes, such as development of new types of batteries.

Acknowledgements

The authors would like to acknowledge funding for this research from the European Community's Seventh Framework Program FP7/2007–2013 under grant agreement No 226943-FLYHY. The Danish Research Council for Natural Sciences (Danscatt) and the Swiss National Science Foundation are also thanked for financial support. Moreover, the work was sup-ported by the Danish National Research Foundation (Centre for Materials Crystallography, DNRF93), the Danish Strategic Research Council (the project Hy-FillFast) and the Carlsberg Foundation. The access to beam time at the MAX-II synchrotron, Lund, Sweden in the research laboratory MAX-lab and at the Swiss-Norwegian Beam Lines (SNBL), European Synchrotron Radia-tion Facility (ESRF), Grenoble, France is gratefully acknowledged. Finally, we thank the Danish Natural Science Research Council, the Danish Technical Science Research Council, and the Carlsberg Foundation for funding to the Instrument Centre for Solid-State NMR Spectroscopy, Aarhus University.

References

1. H. W. Li, Y. Yan, S. Orimo, A. Zu¨ttel and C. M. Jensen, Energies, 2011, 4, 185–214.
2. S. I. Orimo, Y. Nakamori, J. R. Eliseo, A. Zu¨ttel and C. M. Jensen, Chem. Rev., 2007, 107, 4111–4132.
3. L. Schlapbach, Nature, 2009, 460, 809–811.
4. L. Schlapbach and A. Zu¨ttel, Nature, 2001, 414, 353–358.
5. J. Graetz, Chem. Soc. Rev., 2009, 38, 73–82.
6. U.S. Department of Energy, http://www1.eere.energy.gov/ hydrogenandfuelcells/storage/pdfs/targets_onboard_hydro_ storage.pdf.
7. N. Armaroli and V. Balzani, Angew. Chem., Int. Ed., 2007, 46, 52–66.
8. L. H. Rude, T. K. Nielsen, D. B. Ravnsbaek, U. Bo¨senberg, M. B. Ley, B. Richter, L. M. Arnbjerg, M. Dornheim, Y. Filinchuk, F. Besenbacher and T. R. Jensen, Phys. Status Solidi, 2011, 208, 1754–1773.
9. D. B. Ravnsbaek, Y. Filinchuk, R. Cerny´ and T. R. Jensen, Z. Kristallogr., 2010, 225, 557–569.
10. Y. Filinchuk, D. Chernyshov and V. Dmitriev, Z. Kristallogr., 2008, 223, 649–659.
11. V. D'Anna, L. M. L. Daku, H. Hagemann and F. Kubel, Phys. Rev. B: Condens. Matter Mater. Phys., 2010, 82, 024108.
12. H. W. Brinks, A. Fossdal and B. C. Hauback, J. Phys. Chem. C, 2008, 112, 5658–5661.
13. L. C. Yin, P. Wang, X. D. Kang, C. H. Sun and H. M. Cheng, Phys. Chem. Chem. Phys., 2007, 9, 1499–1502.
14. N. Eigen, U. Bo¨senberg, J. Bellosta von Colbe, T. R. Jensen, Cerenius, M. Dornheim, T. Klassen and R. Bormann, Alloys Compd., 2009, 477, 76–80.
15. L. Mosegaard, B. Møller, J.-E. Jørgensen, Y. Filinchuk, Cerenius, J. C. Hanson, E. Dimasi, F. Besenbacher and R. Jensen, J. Phys. Chem. C, 2008, 112, 1299–1303.
16. L. M. Arnbjerg, D. B. Ravnsbaek, Y. Filinchuk, R. T. Vang, Cerenius, F. Besenbacher, J. E. Jørgensen, H. J. Jakobsen and T. R. Jensen, Chem. Mater., 2009, 21, 5772–5782.
17. L. H. Rude, O. Zavorotynska, L. M. Arnbjerg, D. B. Ravnsbaek, R. A. Malmkjaer, H. Grove, B. C. Hauback, Baricco, Y. Filinchuk, F. Besenbacher and T. R. Jensen, Int. J. Hydrogen Energy, 2011, 36, 15664–15672.
18. L. H. Rude, E. Groppo, L. M. Arnbjerg, D. B. Ravnsbaek, Malmkjaer, Y. Filinchuk, M. Baricco, F. Besenbacher and T. R. Jensen, J. Alloys Compd., 2011, 509, 8299–8305.
19. D. B. Ravnsbaek, L. H. Rude and T. R. Jensen, J. Solid State Chem., 2011, 184, 1858–1866.
20. J. Y. Lee, Y.-S. Lee, J.-Y. Suh, J.-H. Shim and Y. W. Cho, Alloys Compd., 2010, 506, 721–727.

21. L. H. Rude, Y. Filinchuk, M. H. Sørby, B. C. Hauback, Besenbacher and T. R. Jensen, J. Phys. Chem. C, 2011, 115, 7768–7777.
22. O. Zavorotynska, M. Corno, E. Pinatel, L. H. Rude, P. Ugliengo, R. Jensen and M. Baricco, Crystals, 2012, 2, 144–158.
23. S. Hino, J. E. Fonneløp, M. Corno, O. Zavorotynska, Richter, M. Baricco, T. R. Jensen, M. H. Sørby and C. Hauback, J. Phys. Chem. C, 2012, 116, 12482–12488.
24. J. E. Olsen, M. H. Sørby and B. C. Hauback, J. Alloys Compd., 2011, 509, L228–L231.
25. M. Corno, E. Pinatel, P. Ugliengo and M. Baricco, J. Alloys Compd., 2011, 509, S679–S683.
26. L. C. Yin, P. Wang, Z. Fang and H. M. Cheng, Chem. Phys. Lett., 2008, 450, 318–321.
27. O. Hideo and F. Kazuo, J. Nucl. Mater., 1977, 64, 37–43.
28. C. W. F. T. Pistorius, Z. Phys. Chem., 1974, 88, 253.
29. Z.-Z. Fang, X.-D. Kang, Z.-X. Yang, G. S. Walker and P. Wang, Phys. Chem. C, 2011, 115, 11839–11845.
30. R. Gosalawit-Utke, J. M. Bellosta von Colbe, M. Dornheim, R. Jensen, Y. Cerenius, C. Bonatto Minella, M. Peschke and R. Bormann, J. Phys. Chem. C, 2010, 114, 10291–10296.
31. R. H. Heyn, I. Saldan, M. H. Sørby, C. Frommen, B. Arstad, M. Bougza, H. Fjellvåg and B. C. Hauback, Phys. Chem. Chem. Phys., 2013, 15, 11226–11230.
32. J. Huot, D. B. Ravnsbaek, J. Zhang, F. Cuevas, M. Latroche and T. R. Jensen, Prog. Mater. Sci., 2013, 58, 30–75.
33. M. J. Frisch, G. W. Trucks, H. B. Schlegel, G. E. Scuseria, Robb, J. R. Cheeseman, G. Scalmani, V. Barone, Mennucci, G. A. Petersson, H. Nakatsuji, M. Caricato, Li, H. P. Hratchian, A. F. Izmaylov, J. Bloino, G. Zheng, L. Sonnenberg, M. Hada, M. Ehara, K. Toyota, R. Fukuda, Hasegawa, M. Ishida, T. Nakajima, Y. Honda, O. Kitao, Nakai, T. Vreven, J. A. Montgomery, J. E. Peralta, Ogliaro, M. Bearpark, J. J. Heyd, E. Brothers, K. N. Kudin, N. Staroverov, R. Kobayashi, J. Normand, K. Raghavachari, Rendell, J. C. Burant, S. S. Lyengar, J. Tomasi, M. Cossi, Rega, J. M. Millam, M. Klene, J. E. Knox, J. B. Cross, Bakken, C. Adamo, J. Jaramillo, R. Gomperts, R. E. Stratmann, O. Yazyev, A. J. Austin, R. Cammi, C. Pomelli, J. W. Ochterski, R. L. Martin, K. Morokuma, V. G. Zakrzewski, G. A. Voth, P. Salvador, J. J. Dannenberg, S. Dapprich, A. D. Daniels, O. Farkas, J. B. Foresman, J. V. Ortiz, J. Cioslowski and D. J. Fox, Gaussian 09, Revision A.1, Gaussian, Inc., Wallingford, CT, USA, 2009.
34. Y. Cerenius, K. Stahl, L. A. Svensson, T. Ursby, A. Oskarsson, Albertsson and A. Liljas, J. Synchrotron Radiat., 2000, 7, 203–208.
35. L. Mosegaard, B. Møller, J. E. Jørgensen, U. Bo¨senberg, Dornheim, J. C. Hanson, Y. Cerenius, G. S. Walker, J. Jakobsen, F. Besenbacher and T. R. Jensen, J. Alloys Compd., 2007, 446–447, 301–305.
36. T. R. Jensen, T. K. Nielsen, Y. Filinchuk, J. E. Jørgensen, Cerenius, E. M. Gray and C. J. Webb, J. Appl. Crystallogr., 2010, 43, 1456–1463.
37. P. Hammersley, S. O. Svensson, M. Hanfland, A. N. Fitch and D. Hausermann, High Pressure Res., 1996, 14, 235–248.
38. J. Rodriguez-Carvajal, Fullprof Suite: LLB Sacley & LCSIM Rennes, France, 2003.
39. J. Skibsted, N. C. Nielsen, H. Bildsøe and H. J. Jakobsen, Magn. Reson., 1991, 95, 88–117.
40. K. J. Gross, R. K. Carrington, S. Barcelo, A. Karkamkar, Pureval, S. Ma, H. C. Zhou, P. Dantzer, K. Ott, T. Burrell, Semeslberger, Y. Pivak, B. Dam and D. Chandra, Recom-mended Best Practices for the Characterization of Storage Properties of Hydrogen Storage Materials, V3-5 U.S. D.O.E. Hydrogen Program document, 2011.
41. L. H. Rude, Y. Filinchuk, U. Filsø, F. Besenbacher, J. Skibsted and T. R. Jensen, 2013, in preparation.
42. R. Cerny´, G. Severa, D. B. Ravnsbaek, Y. Filinchuk, V. d'Anna, H. Hagemann, D. Haase, C. M. Jensen and T. R. Jensen, J. Phys. Chem. C, 2010, 114, 1357–1364.
43. A. C. Stowe, W. J. Shaw, J. C. Linehan, B. Schmid and T. Autrey, Phys. Chem. Chem. Phys., 2007, 9, 1831–1836.
44. R. Caputo, S. Garroni, D. Olid, F. Teixidor, S. Surin˜ach and M. D. Baro´, Phys. Chem. Chem. Phys., 2010, 12, 15093–15100.
45. D. B. Ravnsbaek, Y. Filinchuk, R. Cerny´, M. B. Ley, D. Haase, H. J. Jakobsen, J. Skibsted and T. R. Jensen, Inorg. Chem., 2010, 49, 3801–3809.
46. S. Hayashi and K. Hayamizu, Bull. Chem. Soc. Jpn., 1990, 63, 913–919.
47. L. Seballos, J. Z. Zhang, E. Ro¨nnebro, J. L. Herberg and E. H. Majzoub, J. Alloys Compd., 2009, 476, 446–450.
48. H. M. Maurer, P. C. Schmidt and A. Weiss, J. Mol. Struct., 1977, 41, 111–130.
49. M. H. W. Verkuijlen, P. J. M. van Bentum, E. R. H. van Eck, W. Lohstroh, M. Fichtner and A. P. M. Kentgens, J. Phys. Chem. C, 2009, 113, 15467–15472.
50. P. Carbonnie`re and H. Hagemann, J. Phys. Chem. A, 2006, 110, 9927–9933.
51. J. Urgnani, F. J. Torres, M. Palumbo and M. Baricco, Int. J. Hydrogen Energy, 2008, 33, 3111–3115.
52. M. Paskevicius, M. P. Pitt, C. J. Webb, D. A. Sheppard, U. Filsø, E. M. A. Gray and C. E. Buckley, J. Phys. Chem. C, 2012, 116, 15231–15240.
53. P. Ngene, R. van den Berg, M. H. W. Verkuijlen, K. P. de Jong and P. E. de Jongh, Energy Environ. Sci., 2011, 4, 4108–4115.
54. K. B. Kim, J. H. Shim, Y. W. Cho and K. H. Oh, Chem. Commun., 2011, 47, 9831–9833.
55. Y. Yan, A. Remhof, S.-J. Hwang, H.-W. Li, P. Mauron, S. Orimo and A. Zu¨ttel, Phys. Chem. Chem. Phys., 2012, 14, 6514–6519.
56. O. Friedrichs, A. Remhof, S. Hwang and A. Zu¨ttel, Chem. Mater., 2010, 22, 3265–3268.
57. M. P. Pitt, M. Paskevicius, D. H. Brown, A. S. Drew and C. E. Buckley, J. Am. Chem. Soc., 2013, 135, 6930–6941.